

Recent Advances in Transfer Function-Based Surrogate Optimization for EM Design (Invited)

Wei Liu¹, Feng Feng^{1, *}, and Qi-Jun Zhang²

Abstract—This article provides a review of transfer function-based (TF-based) surrogate optimization for electromagnetic (EM) design. Transfer functions (TF) represent the EM responses of passive microwave components versus frequency. With the assistance of TF, the nonlinearity of the model structure can be decreased. Parallel gradient-based EM optimization technique using TF in rational format and trust region algorithm is introduced first. Following that, we review the EM optimization using adjoint sensitivity-based neuro-TF surrogate, where the neuro-TF modeling method is in pole/residue format. The adjoint sensitivity-based neuro-TF surrogate technique can reach the optimal EM responses solution faster than the existing gradient-based surrogate optimization methods without sensitivity information. As a further advancement, we discuss the multifeature-assisted neuro-TF surrogate optimization technique. With the help of multiple feature parameters, the multifeature-assisted neuro-TF surrogate optimization has a better ability of avoiding local minima and can achieve the optimal EM solution faster than the surrogate optimizations without feature assistance. Three examples are used to verify the above three methods.

1. INTRODUCTION

Electromagnetic (EM)-based optimization and design often requires a large amount of CPU cost to find the optimum design variables. Direct EM optimization is time-consuming to achieve an optimal solution because it usually requires repetitive EM simulations with respect to different geometrical parameters. Efficient EM optimization methods need to be developed to increase the optimization speed.

One way is to use the method of EM inverse modeling by incorporating neural networks. Using the inverse modeling, with the design specifications as input, the design parameters can be directly obtained. Although the optimization time is completely reduced, reverse modeling not only requires the generation of huge data in advance, but also requires the use of complex learning methods such as deep neural networks. A lot of work has been done in EM reverse modeling based on neural network [1–3]. Another way is to accelerate the iteration speed of complex EM responses. Surrogate-based EM optimization techniques can significantly increase the speed of the EM optimization. One of the most efficient surrogate optimization techniques is space-mapping [4–6]. Space-mapping uses the fewest fine model evaluations by exploiting coarse models (e.g., equivalent circuits or empirical) during EM optimization, thereby combining the computational accuracy of fine models with the efficiency of coarse models. Recent efforts on SM techniques have focused on many areas, such as implicit SM [7], aggressive SM [8, 9], output SM [10, 11], neuro-SM [12–16], generalized SM [17], portable SM [18], coarse- and fine-mesh SM [20], SM with adjoint sensitivities [19], and examples of various applications using SM [21–46]. However, most SM techniques require coarse models to be available. To achieve efficient EM optimization without available coarse models, surrogates that use transfer functions (TF)

Received 3 November 2021, Accepted 28 December 2021, Scheduled 31 December 2021

* Corresponding author: Feng Feng (ff@tju.edu.cn).

¹ School of Microelectronics, Tianjin University, Tianjin 300072, China. ² Department of Electronics, Carleton University, Ottawa, ON, K1S5B6, Canada.

are utilized. As a further research, surrogates combine neural networks and transfer functions (neuro-transfer function (neuro-TF)) have also been developed for microwave passive components [47–51]. The neuro-TF methods for EM optimization address the situation where equivalent circuits models are unavailable [47, 48]. The TF can express EM responses of passive components versus frequency. Sensitivity analysis has also been involved in neuro-TF optimization to increase the modeling accuracy and optimization efficiency [49]. In [50] and [51], parallel computation has been researched in surrogate optimization. These optimization methods use gradient-based algorithm with TF/neuro-TF models as surrogates. When the initial EM response is far away from the design specifications, algorithms in [50] and [51] can easily fall into local minima. To solve this problem, feature-based EM optimization techniques have been introduced [52, 53]. With the feature parameters to assist EM optimization, the ability of avoiding to fall into local minima has been increased. The feature-based optimization addresses a situation where the initial EM response has an incorrect number of feature frequencies [54]. To address this situation where the EM response does not have clearly identifiable features, a surrogate optimization exploiting the assisted feature frequencies extracted from neuro-TF is presented [55].

In this article, recent advances in TF-based surrogate optimization for EM design are presented, including the parallel gradient-based EM optimization technique using transfer function and trust region algorithm, an advancement in parallel EM optimization using adjoint sensitivity-based neuro-TF surrogate, and a further advancement in multifeature-assisted neuro-TF surrogate-based EM optimization technique. Compared with the gradient-based surrogate optimization without adjoint sensitivity, the accurate surrogate models with a larger valid design variables range can be obtained accurately and efficiently by using adjoint sensitivity for surrogate optimization. The sensitivities calculated using the developed surrogate model are much more accurate [56]. The accurate gradients can improve the quality of surrogate optimal EM solution in each iteration. Since the gradients are sufficiently accurate, and the surrogate model is valid in a large neighborhood, the adjoint sensitivity-based neuro-TF surrogate technique achieves speedup in the overall optimization process. The new multifeature-assisted neuro-TF surrogate-based EM optimization technique utilizes multiple feature parameters to help move the passband of the filter response into the range of design specifications. When the feature parameters of EM responses are not clearly identifiable, the pole-residue-based neuro-TF is introduced to assist extracting the multiple feature parameters. A new trust-region updating algorithm is derived to achieve the optimization convergence. The new multifeature-assisted surrogate optimization has a better ability of avoiding local minima than the surrogate optimizations without feature assistance and can speed up to achieve the optimal solution [57].

2. SURROGATE OPTIMIZATION COMBINING TRANSFER FUNCTION IN RATIONAL FORMAT WITH TRUST REGION ALGORITHMS

2.1. Transfer Function in Rational Format and Trust Region Algorithms

The vector-fitting approach [58] is used to extract the coefficients of the TF from the EM responses. Let R_s represent the TF output. The TF in rational format is formulated [50]

$$R_s(s) = \frac{\sum_{i=0}^N a_i s^i}{1 + \sum_{i=1}^N b_i s^i} \quad (1)$$

where s is the Laplace frequency variable; a_i and b_i are the coefficients of the rational TF; N is the order of the transfer function; TF to represent the EM behavior. The surrogate model, which is valid across the all trust region (DOE sample space), provides the output response R_s .

Conventional EM optimization is generally based on single fine model evaluations per iteration. However, trust region algorithm uses a set of fine model evaluations in a relatively larger neighborhood around a central point to provide rich information in estimating the direction for the next iteration update. These fine model evaluations along with the central point are used to predict the overall behavior in the region of interest. The central point is updated after each iteration of the optimization

using trust region framework formulas. From equations in [50], the coefficients of the TF are dependent only on the design variables. \mathbf{w}_r represents vector weighting factors of each coefficient of the numerator or denominator. The values of \mathbf{w}_r are optimized so that the error between the surrogate model response and the fine model response is minimized, and \mathbf{w}_* for i th iteration is formulated as [50]

$$\mathbf{w}^* = \arg \min_{\mathbf{w}} \sum_{k=1}^{N_s} \sum_{\omega \in \Omega} \|R_s - R_f\| = \arg \min_{\mathbf{w}} \sum_{k=1}^{N_s} \sum_{\omega \in \Omega} \|H - R_f\| \quad (2)$$

where ω represents the complete frequency points used for the fine model response, N_s the number of samples in the trust region, and R_f the output response of the fine model. An accurate surrogate model match is obtained not only at the DOE samples in the trust region, but also across the whole trust region.

2.2. Surrogate Model Optimization and Trust Region Update

The surrogate optimization combining transfer function in rational format with trust region technique is formulated as distribution of multiple data samples using sampling techniques, computation using parallel processors, optimization update using trust region framework. The orthogonal sampling is used for generating multiple sample points where the subspaces are sampled with the same density and are orthogonal. The orthogonal sampling around the central point enables the surrogate model to be valid in relatively large neighborhood compared to star distribution and also uses far fewer sampling points than full-grid distribution [47]. Once the trust region is defined, the design of experiments (DOE) [47] sampling strategy is used to generate a set of samples around the central point in each iteration of the optimization process. Fig. 1 shows the design of experiments (DOE) sampling strategy used to generate sample points around a central point. When the optimization process moves, the central point moves to a new optimization area. All the other DOE sample points move along with the central point. Therefore, the values of samples change from iteration to iteration. The trust region changes from iteration to iteration based on trust radius δ^{new} . The control index r_a [50] determines whether the trust radius has to be expanded from the previous iteration or remain unchanged, as formulate [50]

$$\delta^{\text{new}} = \begin{cases} c_1 \delta^{(i)}, & r_a < 0.1 \\ \min(c_2 \delta^{(i)}, \Delta^{\text{max}}), & r_a > 0.75 \\ \delta^{(i)}, & \text{Otherwise} \end{cases} \quad (3)$$

where Δ^{max} is the maximum limit for each design variable. $c_1 = 0.69$ and $c_2 = 1.3$. Parallel computational approach is used for fine model evaluations over multiple samples. Parallel computational approach is implemented to accelerate data generation.

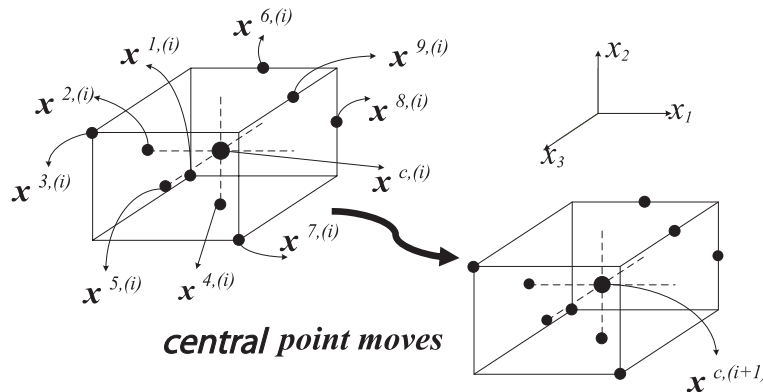


Figure 1. Illustration of orthogonal arrays (a type of DOE) sampling technique to generate multiple sample points in the trust region [50].

3. SENSITIVITY-ANALYSIS-BASED NEURO-TF SURROGATE OPTIMIZATION

3.1. Structure of the Sensitivity-Analysis-Based Neuro-TF Model

An advanced method for building neuro-TF models with less training data is sensitivity analysis. Fig. 2 shows the structure of a sensitivity-analysis-based neuro-TF model. The sensitivity-analysis-based neuro-TF model consists of two sub-models, i.e., the neuro-TF model and adjoint neuro-TF model based on sensitivity analysis [56]. Two sub-models share the same inputs \mathbf{x} . The sensitivities of the outputs \mathbf{y}_s of original neuro-TF model with respect to the inputs \mathbf{x} , denoted as $\tilde{\mathbf{y}}_s$, are defined as the outputs of the adjoint neuro-TF model. The original neural networks and the adjoint neural networks map the relationship between the sensitivities of TF parameters and geometrical parameters. The response $H(s)$ of the pole-residue-based TF is formulated as follows [56]

$$H(s) = \sum_{i=1}^N \frac{r_i}{s - p_i} \quad (4)$$

where p_i and r_i represent the poles and residues in the TF, and N represents the order of the TF. Vector-fitting [58] is used to extract the coefficients p_i and r_i .

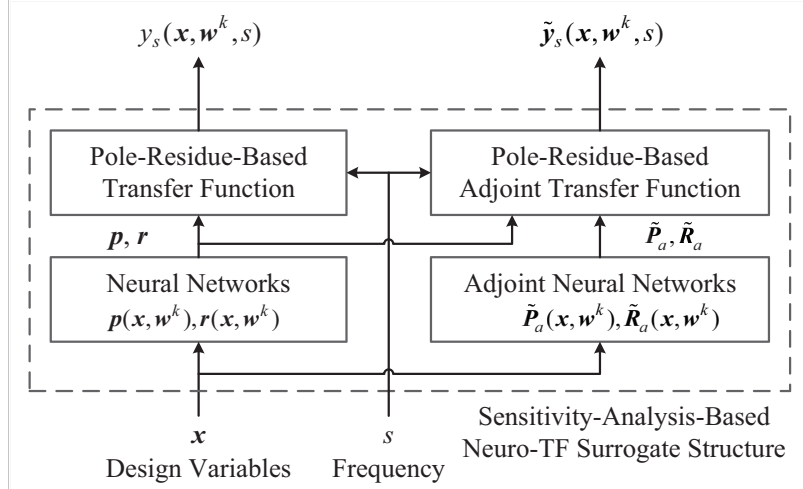


Figure 2. The general structure of the sensitivity-analysis-based neuro-TF model. The model consists of the neuro-TF model and the adjoint neuro-TF model [55].

3.2. Two-Stage Training for the Sensitivity-Analysis-Based Neuro-TF Model

The sensitivity-analysis-based model is trained through a two-stage training process, including preliminary training and refinement training.

In the first stage training, the original and adjoint neural networks are trained simultaneously. Let $\hat{\mathbf{c}}_k$ and $\hat{\mathbf{A}}_k$ represent the data of transfer function parameters and their sensitivities with respect to \mathbf{x} , respectively. $(\mathbf{x}_k, \hat{\mathbf{c}}_k)$ represents the training data for the original neural networks. $(\mathbf{x}_k, \hat{\mathbf{A}}_k)$ represents the training data for the adjoint neural networks. $\mathbf{c}(\mathbf{x}, \mathbf{w})$ is a vector including the outputs of the neural networks, i.e., TF parameters. The error function for the first stage training is formulated as [56]

$$E_{Pre}(\mathbf{w}) = \frac{1}{2n_s} \sum_{k=1}^{n_s} \|\mathbf{c}(\mathbf{x}_k, \mathbf{w}) - \hat{\mathbf{c}}_k\|^2 + \frac{1}{2n_s} \sum_{k=1}^{n_s} \left\| \frac{\partial \mathbf{c}(\mathbf{x}_k, \mathbf{w})}{\partial \mathbf{x}^T} - \hat{\mathbf{A}}_k \right\|_F^2 \quad (5)$$

where $\|\cdot\|$ and $\|\cdot\|_F$ represent L_2 norm and Frobenius norm; n_s represents the number of training samples.

The second-stage training is performed to refine the overall model. $(\mathbf{x}_k, \mathbf{d}_k)$ and $(\mathbf{x}_k, \mathbf{d}'_k)$ represent the training data for original and adjoint neuro-TF models, respectively. The error function of the refinement training is formulated as [56]

$$E_{Tr}(\mathbf{w}) = E_{orig}(\mathbf{w}) + E_{adj}(\mathbf{w}) = \frac{1}{2n_s} \sum_{k=1}^{n_s} \sum_{j=1}^{n_y} a_j \|y_j(\mathbf{x}_k, \mathbf{w}) - d_{k,j}\|^2 + \frac{1}{2n_s} \sum_{k=1}^{n_s} \sum_{j=1}^{n_y} \sum_{i=1}^{n_x} b_{j,i} \left\| \frac{\partial y_j(\mathbf{x}_k, \mathbf{w})}{\partial x_i} - d'_{k,j,i} \right\|^2 \quad (6)$$

where E_{orig} represents the training error between the original neuro-TF model and the EM simulation data. E_{adj} represents the training error between the EM sensitivity data and the adjoint neuro-TF model. n_y and n_x are the numbers of elements of \mathbf{y} and \mathbf{x} , respectively. n_s is the total number of training samples. a_j and $b_{j,i}$ are the weighting parameters for the original neuro-TF model and the adjoint neuro-TF model. $d_{k,j}$ represents the EM simulation data of the k th sample for the j th output. $d'_{k,j,i}$ is the EM sensitivity data of the k th sample for the j th output with respect to the i th input. The overall training process terminates until the total training error is smaller than a defined error threshold. The original neuro-TF model has accurate sensitivity information after overall training. Because the adjoint neuro-TF model is only used for the training process, the final model is simple and can be further used in optimization design.

3.3. Optimization Formulation Using Adjoint-Sensitivity Based Neuro-TF Surrogate

Optimization formulations for trained surrogate model are used to minimize the sum of the squared differences between the surrogate model and the fine model, which is formulated as [56]

$$E^k(\mathbf{w}) = \alpha E_o^k(\mathbf{w}) + \beta E_a^k(\mathbf{w}) = \alpha \sum_{i=1}^{n_s} \sum_{j=1}^{n_f} \left\| y_s(\mathbf{x}_i^k, \mathbf{w}, s_j) - y_f(\mathbf{x}_i^k, s_j) \right\|^2 + \beta \sum_{i=1}^{n_s} \sum_{j=1}^{n_f} \left\| \tilde{y}_s(\mathbf{x}_i^k, \mathbf{w}, s_j) - \tilde{y}_f(\mathbf{x}_i^k, s_j) \right\|^2 \quad (7)$$

$$\mathbf{w}^k = \arg \min_w E^k(\mathbf{w}) \quad (8)$$

where y_f and \tilde{y}_f represent the fine model EM response and the adjoint EM sensitivities, respectively. n_s represents the number of fine models used. E^k represents the training error of the original and adjoint neuro-TF models in the k th optimization iteration, E_o^k the training error of the neuro-TF models, E_a^k the training error of the adjoint neuro-TF models, n_f the number of frequencies, and α and β represent the weighting parameters. w_k are the optimal parameters of the neuro-TF at the k th iteration. The accurate sensitivity information leads to speedup of the surrogate optimization and reduce the number of iterations.

4. FEATURE-ASSISTED NEURO-TF SURROGATE OPTIMIZATION

Further, feature parameters are used to speed up surrogate optimization for EM design. Usually, the feature frequency points and frequency responses at specific locations are used as feature parameters [57]. The feature parameters can avoid local minima and help drive the optimization to reach the optimal EM solution faster. The feature frequencies and EM responses at locations of design requirement are usually used as feature parameters. Fig. 3 shows the structure of the feature-assisted neuro-TF model. The pole-residue-based TF is used in the feature-assisted neuro-TF. The feature parameters are the outputs of neural networks in the feature-assisted neuro-TF model.

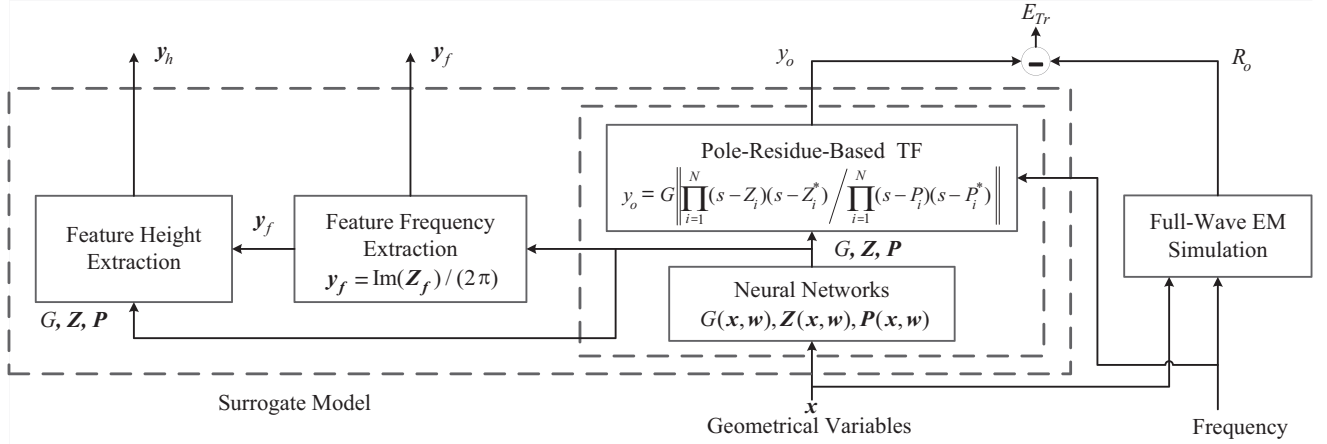


Figure 3. Structure of the feature-assisted neuro-TF model [57]. The TF transfer parameters are poles/residues/gain.

When the neuro-TF model is well trained, we can further extract the multiple feature parameters to assist the surrogate optimization, including feature frequencies y_l^f and feature heights y_h . The feature frequencies are related to the imaginary parts of residues of the TF. The extracting formulation is [57]

$$y_l^f(\mathbf{x}, \mathbf{w}) = \frac{\text{Im}(Z_{Q_l}(\mathbf{x}, \mathbf{w}))}{2\pi}, \quad l = 1, 2, \dots, N_f \quad (9)$$

where $l = 1$,

$$Q_l = \arg \min_{q \in \{1, \dots, N_k\}} \left\{ \sum_{j=1}^{n_s} \|\text{Re}(z_q^j)\| \right\} \quad (10)$$

$l \geq 2$,

$$Q_l = \arg \min_{\substack{q \in \{1, \dots, N_k\} \\ q \notin \{Q_1, \dots, Q_{l-1}\}}} \left\{ \sum_{j=1}^{n_s} \|\text{Re}(z_q^j)\| \right\} \quad (11)$$

where z_q^j is the data of the q th residue of the TF for the j th geometrical sample. n_s represents the number of training samples. y_h is the magnitude of the S -parameter which is located at the midfrequencies between two feature frequencies. After feature parameter extraction, we perform the surrogate-based EM optimization using the feature-assisted neuro-TF model [57].

5. SURROGATE OPTIMIZATION APPLICATIONS IN PASSIVE MICROWAVE COMPONENTS

5.1. Transfer Function-Based Surrogate Optimization for Inter-Digital Band-Pass Filter

An inter-digital band-pass filter example [50] is illustrated in Fig. 4. g is the gap between the end of the resonator and the cavity wall. l_r is the length of the resonator. s_1 , s_2 , and s_3 are the spacing between the resonators. The model has four input geometrical variables, i.e., $\mathbf{x} = [g \ s_1 \ s_2 \ s_3]^T$. The model output is the magnitude of S_{11} . The initial central point is selected by designer experience of the problem in case of the corresponding fine model response too far away from the optimal solution.

For this application, the design specification is $|S_{11}| \leq -30$ dB in the frequency range of 1.3 GHz–1.8 GHz. The initial point for optimization is $\mathbf{x}^0 = [0.423 \ 0.125 \ 0.247 \ 0.232]^T$ (mm). The optimization is performed using the surrogate optimization combining transfer function in rational format with trust region algorithms. The EM data generation and optimization verification are performed using *HFSS*. The optimized geometrical solution $\mathbf{x}^6 = [3.0128 \ 0.728381 \ 1.92592 \ 2.28048]^T$ (mm) is achieved after six

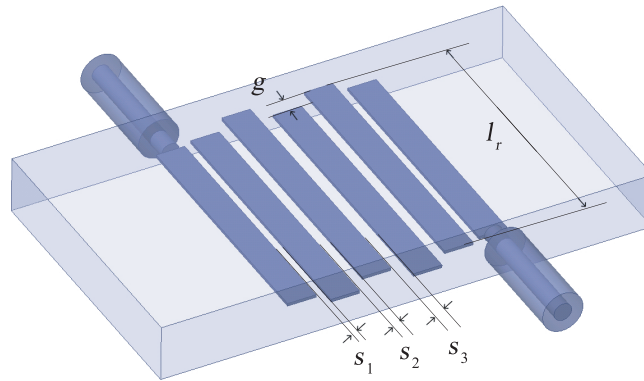


Figure 4. Structure of a inter-digital band-pass filter [50].

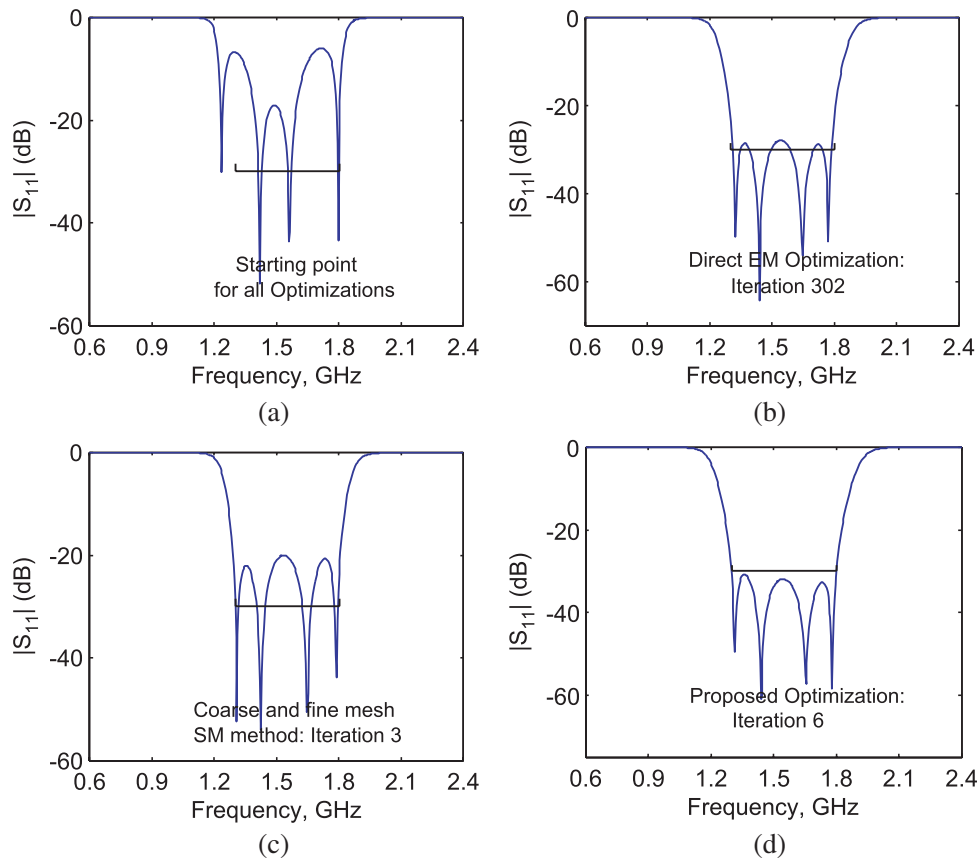


Figure 5. Comparison of three different optimization methods [50].

optimization iterations. Fig. 5(a) and Fig. 5(d) show the fine model response at the initial and final central point. Coarse and fine mesh space mapping optimization method is used to optimize this filter for comparison. Fig. 5(c) shows the optimal solution obtained after three iterations exploiting coarse and fine mesh method. For a further comparison, EM optimization of this filter using HFSS internal optimization feature is performed. The direct EM optimization method uses HFSS’s built-in gradient based quasi-Newton optimization algorithm. Fig. 5(b) shows the final optimal point obtained that needs 302 fine model evaluations using direct EM optimization.

Figure 6 shows the values of the objective function for the surrogate optimization combining TF in

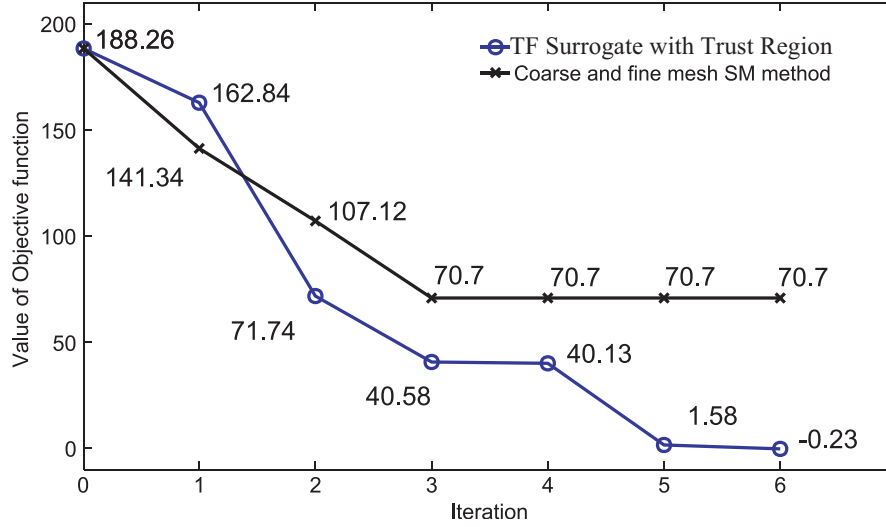


Figure 6. Values of objective function of different methods for the inter-digital band-pass filter [50].

rational format with trust region and coarse and fine mesh SM optimization. The surrogate optimization combining transfer function in rational format with trust region algorithm converges to the optimal solution and has high parallel efficiency even with different numbers of design variables.

5.2. Sensitivity-Analysis-Based Neuro-TF in Surrogate Optimization of Four-Pole Waveguide Filter

For this example, the sensitivity-analysis-based neuro-TF algorithm is used to illustrate the optimization of a four-pole waveguide filter example [56], as shown in Fig. 7. The input and output waveguides and resonant cavities are WR-75 waveguides, $a = 19.05$ mm and $b = 9.525$ mm. h_1 , h_2 , and h_3 are the heights of posts in the coupling windows. h_{c1} and h_{c2} are the heights of the posts in the resonant cavities. The thickness of the coupling windows is 2 mm. Fig. 8 shows the structure of sensitivity-analysis-based neuro-TF model for the four-pole waveguide filter. In this application, pole-residue-based TF is used. $\mathbf{x} = [h_1 \ h_2 \ h_3 \ h_{c1} \ h_{c2}]^T$ are the input geometrical variables of the model. The magnitude of S_{11} and its sensitivities with respect to five design variables are the model outputs. The model is developed using *NeuroModelerPlus* software.

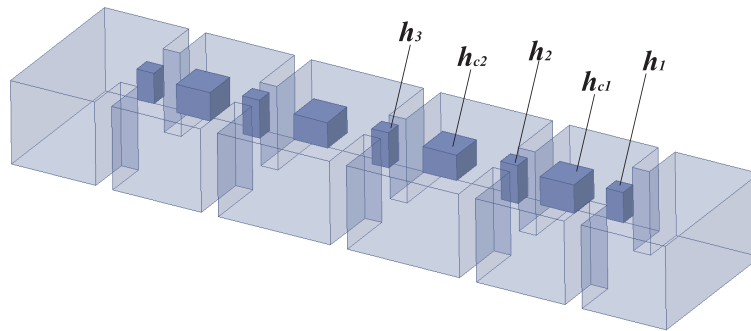


Figure 7. The structure of the four-pole waveguide filter [56].

The design specification is $|S_{11}| \leq -26$ dB in the range of 10.85–1.15 GHz. The initial point for optimization is $\mathbf{x}^0 = [3.0 \ 4.0 \ 3.5 \ 3.3 \ 3.0]^T$ (mm). The optimization is performed using the sensitivity-analysis-based neuro-TF algorithm. The EM data generation and optimization verification are performed using *HFSS*. The optimized geometrical solution $\mathbf{x}^6 = [3.524 \ 4.231 \ 3.726 \ 3.255 \ 2.963]^T$

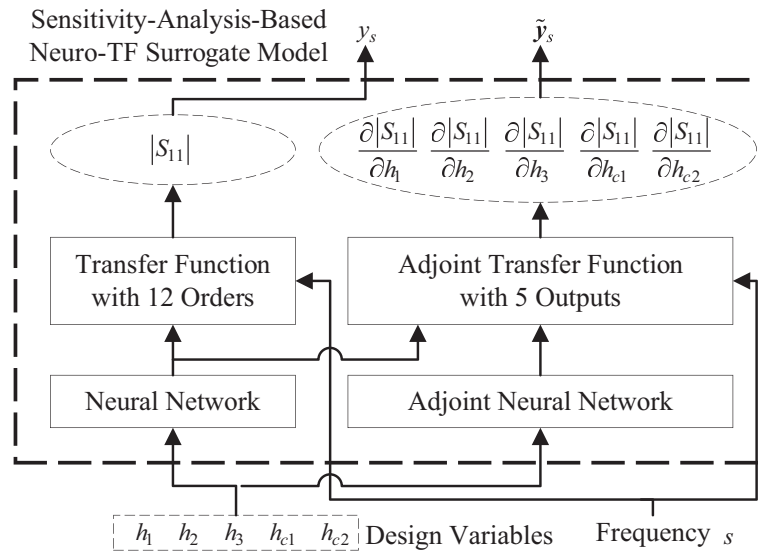


Figure 8. Structure of the adjoint-sensitivity-based neuro-TF model for surrogate optimization [56].

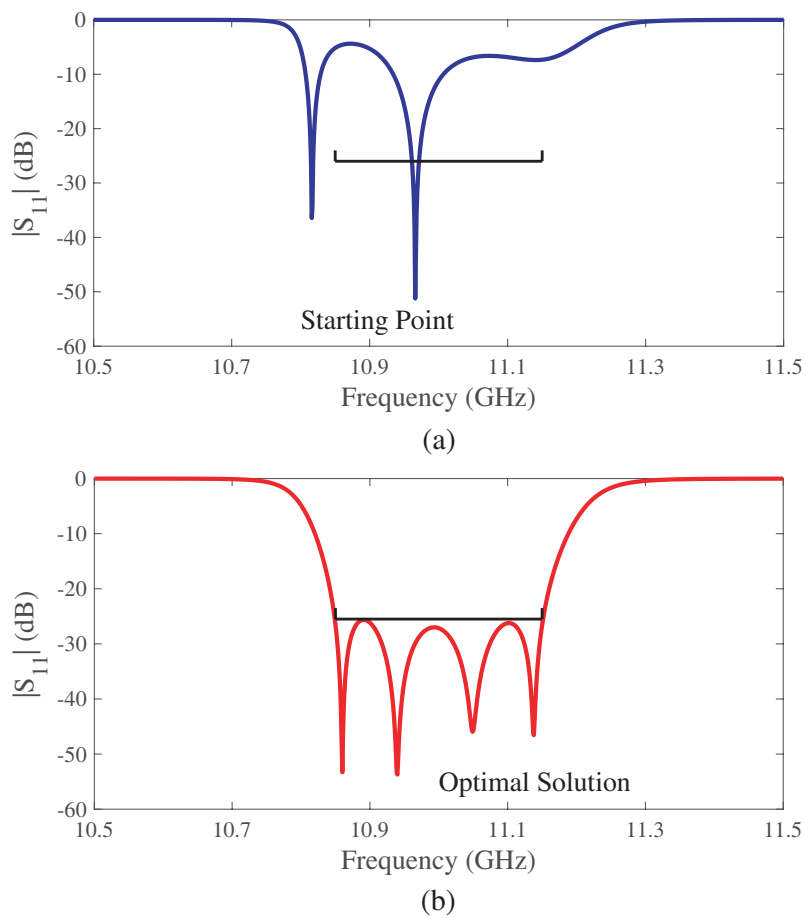


Figure 9. EM responses of the EM optimization using the adjoint-sensitivity-based neuro-TF surrogate for initial iteration and sixth iteration [56].

(mm) is achieved after six optimization iterations. Fig. 9 shows the EM responses of the filter at the initial point and at the optimized geometrical solution using the sensitivity-analysis-based neuro-TF algorithm. Fig. 10 and Fig. 11 compare the outputs and sensitivities respectively from the neuro-TF models trained with less data and more data, the sensitivity-analysis-based neuro-TF model trained with less data, and EM data evaluated at one test sample. Even if the model is trained with less training data, the sensitivity-analysis-based neuro-TF model can achieve accurate modeling and provide accurate sensitivity information.

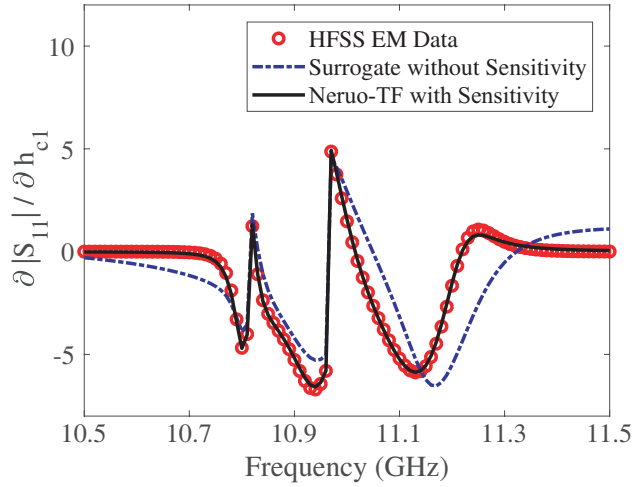


Figure 10. Comparison of the sensitivities of the neuro-TF models trained with less/more data, the sensitivity-analysis-based neuro-TF model trained with less data and HFSS EM sensitivity data at one sample [56].

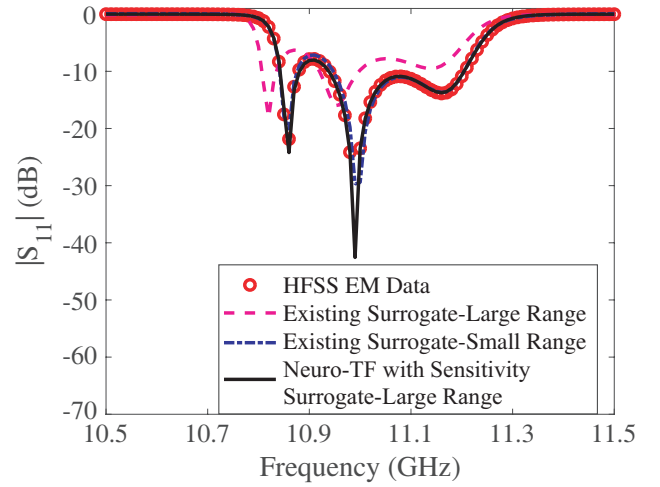


Figure 11. Comparison of S_{11} of the neuro-TF models trained with less/more data, the sensitivity-analysis-based neuro-TF model trained with less data and HFSS EM data [56].

5.3. EM Structural Design of Microwave Cavity Filter Using Feature-Assisted Neuro-TF

The feature-assisted neuro-TF technique is verified by surrogate EM optimization of a microwave cavity filter example [57], as shown in Fig. 12, where H_{c1} , H_{c2} , and H_{c3} are the heights of the large cylinders positioned at the cavity centers; W_1 , W_2 , W_3 , and W_4 are the iris widths for each section. The model

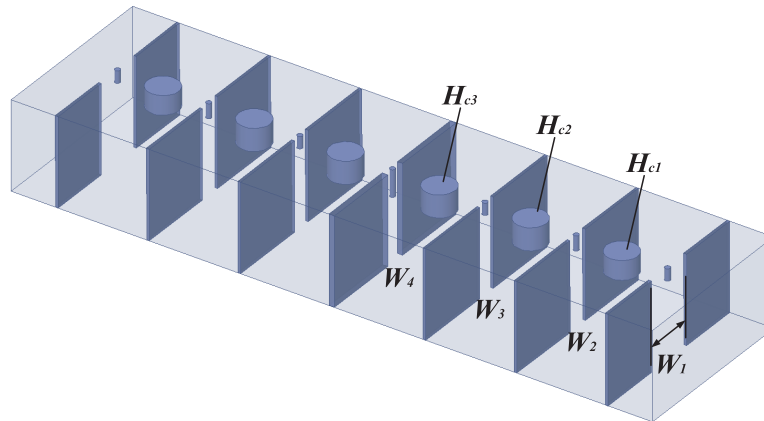


Figure 12. Structure of the interdigital bandpass filter which has five geometrical variables for EM optimization [57].

has seven input geometrical variables, i.e., $\mathbf{x} = [H_{c1} H_{c2} H_{c3} W_1 W_2 W_3 W_4]^T$. The model outputs contain not only the magnitude of S_{11} , but also two sets of feature parameters (feature frequencies and feature heights) from the filter response. The feature frequencies are the imaginary parts of the TF residues. The feature heights are the magnitudes of the TF responses at the mid-frequencies between two feature frequencies. The feature-assisted neuro-TF model is performed using *NeuroModelerPlus* software.

The design specification is $|S_{11}| \leq -20$ dB in the range of 703–713 MHz. The initial point for

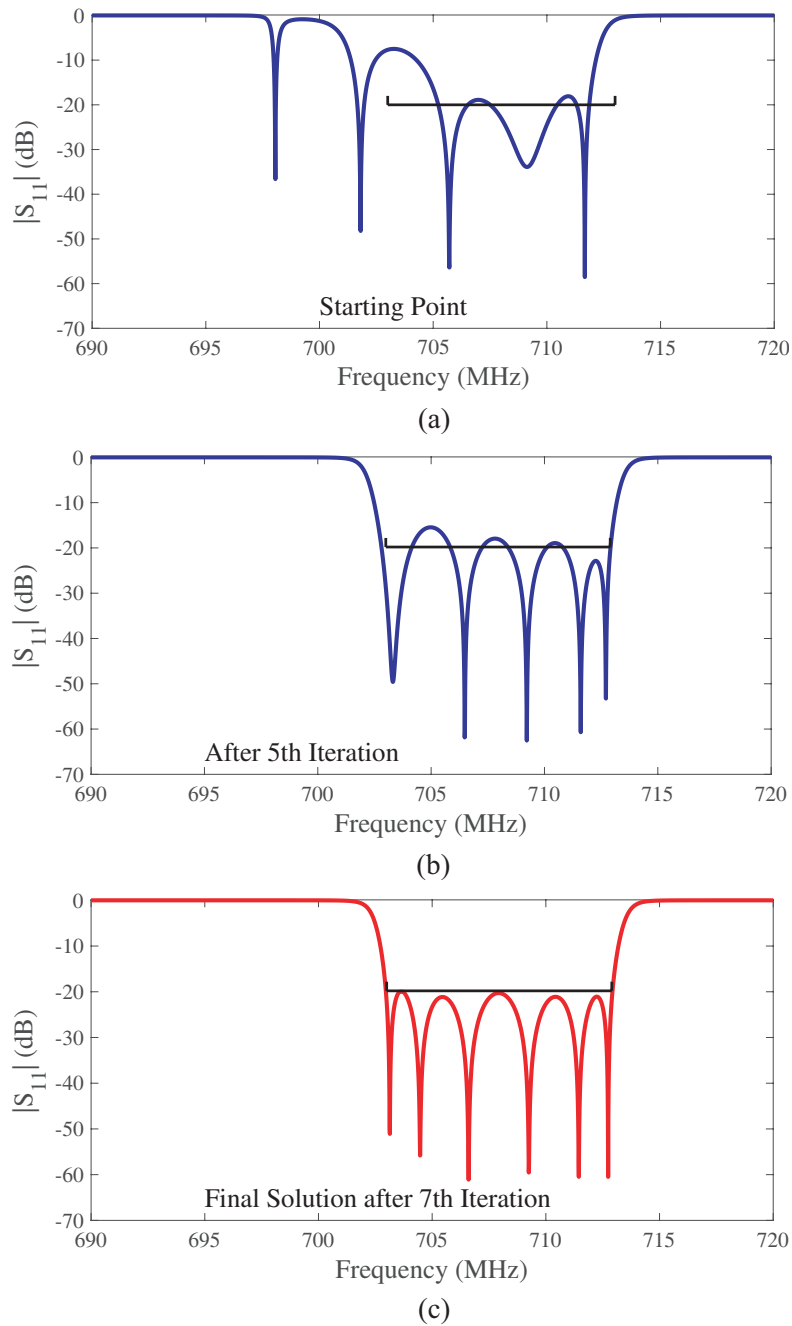


Figure 13. EM responses of the multifeature-assisted surrogate optimization. (a) EM response at the starting point. (b) EM responses at fifth iteration. (c) EM responses at the final solution after seven iterations [57].

optimization is $\mathbf{x}^0 = [43 \ 50.5 \ 50.5 \ 115 \ 51 \ 50 \ 55]^T$ (mm). The optimization is performed using the feature-assisted neuro-TF method. The EM data generation and optimization verification are performed using *HFSS*. The optimized geometrical solution $\mathbf{x}^7 = [42.072 \ 50.343 \ 50.473 \ 115.78 \ 50.123 \ 44.179 \ 47.612]^T$ (mm) is achieved after seven optimization iterations. Fig. 13 shows the EM responses of the filter at the initial point, after the 7th iteration, and at the optimal design solution using the feature-assisted neuro-TF algorithm [57]. When the response at the initial point is far away from the design specifications, the optimization with the assistance of feature parameters can have better chances to avoid the local minima than the optimization without feature assistance.

6. CONCLUSION

TF-based approaches for fast surrogate optimization have been described when geometrical parameters need to be repetitively changed for EM design. Trust-region based optimization algorithm combining TF speeds up optimization process without coarse models. Further, Neuro-TF techniques are used for high-level EM optimization with repetitive design variations. The adjoint-sensitivity-based neuro-TF surrogate is used for parallel gradient-based EM optimization. Since the surrogate model is valid in a large range, and the sensitivities are much accurate, the adjoint-sensitivity-based neuro-TF surrogate optimization has achieved the optimal solution faster than the existing surrogate optimization without sensitivity information. The multifeature-assisted surrogate-based EM optimization for filter design has been introduced to address the situations that the EM response of the initial point for the optimization is far away from the design specifications. These methods have achieved a further EM optimization speedup over the existing surrogate EM optimization methods.

We have focused on a review of TF-based surrogate optimization approaches of passive microwave components. One possible future direction is to further expand the range of optimizable parameters of these methods. That is, when the range of optimizable parameters becomes larger, the applicability of these methods is still maintained. To achieve this goal may need to solve some new problems. A second possible direction is to expand these methods to calculate more EM samples at the same time, especially when the design space increases with the increase in parameters dimensionality. These will further increase the application value of TF-based surrogate optimization methods for EM design.

REFERENCES

1. Zhang, C., J. Jin, W. Na, Q. J. Zhang, and M. Yu, "Multivalued neural network inverse modeling and applications to microwave filters," *IEEE Trans. Microw. Theory Tech.*, Vol. 66, No. 8, 3781–3797, Aug. 2018.
2. Jin, J., C. Zhang, F. Feng, W. Na, J. Ma, and Q. J. Zhang, "Deep neural network technique for high-dimensional microwave modeling and applications to parameter extraction of microwave filters," *IEEE Trans. Microw. Theory Tech.*, Vol. 67, No. 10, 4140–4155, Oct. 2019.
3. Wei, Z. and X. Chen, "Uncertainty quantification in inverse scattering problems with Bayesian convolutional neural networks," *IEEE Trans. Antennas Propag.*, Vol. 69, No. 6, 3409–3418, Jun. 2021.
4. Bandler, J., M. Ismail, J. Rayas-Sanchez, and Q.-J. Zhang, "Neuromodeling of microwave circuits exploiting space-mapping technology," *IEEE Trans. Microw. Theory Tech.*, Vol. 47, No. 12, 2417–2427, Dec. 1999.
5. Bandler, J., Q. Cheng, S. Dakroury, A. Mohamed, M. Bakr, K. Madsen, and J. Sondergaard, "Space mapping: The state of the art," *IEEE Trans. Microw. Theory Tech.*, Vol. 52, No. 1, 337–361, Jan. 2004.
6. Koziel, S., Q. S. Cheng, and J. W. Bandler, "Space mapping," *IEEE Microw. Mag.*, Vol. 9, 105–122, Dec. 2008.
7. Bandler, J., Q. Cheng, N. Nikolova, and M. Ismail, "Implicit space mapping optimization exploiting preassigned parameters," *IEEE Trans. Microw. Theory Tech.*, Vol. 52, No. 1, 378–385, Jan. 2004.

8. Rayas-Sanchez, J. E., "Power in simplicity with asm: Tracing the aggressive space mapping algorithm over two decades of development and engineering applications," *IEEE Microw. Mag.*, Vol. 17, No. 4, 64–76, Apr. 2016.
9. Sans, M., J. Selga, P. Vlez, A. Rodriguez, J. Bonache, V. E. Boria, and F. Martn, "Automated design of common-mode suppressed balanced wideband bandpass filters by means of aggressive space mapping," *IEEE Trans. Microw. Theory Tech.*, Vol. 63, No. 12, 3896–3908, Dec. 2015.
10. Koziel, S., J. W. Bandler, and K. Madsen, "Space mapping with adaptive response correction for microwave design optimization," *IEEE Trans. Microw. Theory Tech.*, Vol. 57, No. 2, 478–486, Feb. 2009.
11. Ayed, R. B., J. Gong, S. Brisset, F. Gillon, and P. Brochet, "Three-level output space mapping strategy for electromagnetic design optimization," *IEEE Microw. Mag.*, Vol. 48, No. 2, 671–674, Feb. 2012.
12. Devabhaktuni, V., B. Chattaraj, M. Yagoub, and Q.-J. Zhang, "Advanced microwave modeling framework exploiting automatic model generation, knowledge neural networks, and space mapping," *IEEE Trans. Microw. Theory Tech.*, Vol. 51, No. 7, 1822–1833, Jul. 2003.
13. Rayas-Sanchez, J., "Em-based optimization of microwave circuits using artificial neural networks: The state-of-the-art," *IEEE Trans. Microw. Theory Tech.*, Vol. 52, No. 1, 420–435, Jan. 2004.
14. Rayas-Sanchez, J., F. Lara-Rojo, and E. Martinez-Guerrero, "A linear inverse space-mapping (LISM) algorithm to design linear and nonlinear RF and microwave circuits," *IEEE Trans. Microw. Theory Tech.*, Vol. 53, No. 3, 960–968, Mar. 2005.
15. Zhang, L., J. Xu, M. Yagoub, R. Ding, and Q.-J. Zhang, "Efficient analytical formulation and sensitivity analysis of neuro-space mapping for nonlinear microwave device modeling," *IEEE Trans. Microw. Theory Tech.*, Vol. 53, No. 9, 2752–2767, Sep. 2005.
16. Zhang, L., Q.-J. Zhang, and J. Wood, "Statistical neuro-space mapping technique for large-signal modeling of nonlinear devices," *IEEE Trans. Microw. Theory Tech.*, Vol. 56, No. 11, 2453–2467, Nov. 2008.
17. Koziel, S., J. Bandler, and K. Madsen, "A space-mapping framework for engineering optimization theory and implementation," *IEEE Trans. Microw. Theory Tech.*, Vol. 54, No. 10, 3721–3730, Oct. 2006.
18. Zhang, L., P. H. Aaen, and J. Wood, "Portable space mapping for efficient statistical modeling of passive components," *IEEE Trans. Microw. Theory Tech.*, Vol. 60, No. 3, 441–450, Mar. 2012.
19. Koziel, S., S. Ogurtsov, J. W. Bandler, and Q. S. Cheng, "Reliable space-mapping optimization integrated with em-based adjoint sensitivities," *IEEE Trans. Microw. Theory Techn.*, Vol. 61, No. 10, 3493–3502, Oct. 2013.
20. Feng, F., C. Zhang, V.-M.-R. Gongal-Reddy, Q.-J. Zhang, and J. Ma, "Parallel space-mapping approach to EM optimization," *IEEE Trans. Microw. Theory Techn.*, Vol. 62, No. 5, 1135–1148, May 2014.
21. Ros, J., P. Pacheco, H. Gonzalez, V. Esbert, C. Martin, M. Calduch, S. Borrás, and B. Martinez, "Fast automated design of waveguide filters using aggressive space mapping with a new segmentation strategy and a hybrid optimization algorithm," *IEEE Trans. Microw. Theory Techn.*, Vol. 53, No. 4, 1130–1142, Apr. 2005.
22. Ismail, M., D. Smith, A. Panariello, Y. Wang, and M. Yu, "Em-based design of large-scale dielectric-resonator filters and multiplexers by space mapping," *IEEE Trans. Microw. Theory Techn.*, Vol. 52, No. 1, 386–392, Jan. 2004.
23. Wu, K.-L., Y.-J. Zhao, J. Wang, and M. Cheng, "An effective dynamic coarse model for optimization design of LTCC RF circuits with aggressive space mapping," *IEEE Trans. Microw. Theory Techn.*, Vol. 52, No. 1, 393–402, Jan. 2004.
24. Amari, S., C. LeDrew, and W. Menzel, "Space-mapping optimization of planar coupled-resonator microwave filters," *IEEE Trans. Microw. Theory Techn.*, Vol. 54, No. 5, 2153–2159, May 2006.
25. Dorica, M. and D. Giannacopoulos, "Response surface space mapping for electromagnetic optimization," *IEEE Microw. Mag.*, Vol. 42, No. 4, 1123–1126, Apr. 2006.

26. Bandler, J. W., M. A. Ismail, and J. E. Rayas-Sanchez, "Expanded space-mapping EM-based design framework exploiting preassigned parameters," *IEEE Trans. Circuits Syst. I, Fundam. Theory Appl.*, Vol. 49, No. 12, 1833–1838, Dec. 2002.
27. Bandler, J. W., D. M. Hailu, K. Madsen, and F. Pedersen, "A space mapping interpolating surrogate algorithm for highly optimized EM-based design of microwave devices," *IEEE Trans. Microw. Theory Techn.*, Vol. 52, No. 11, 2593–2600, Nov. 2004.
28. Ayed, R. B., J. Gong, S. Brisset, F. Gillon, and P. Brochet, "Three-level output space mapping strategy for electromagnetic design optimization," *IEEE Trans. Magn.*, Vol. 48, No. 2, 671–674, Feb. 2012.
29. Zhang, L., J. Xu, M. C. E. Yagoub, R. Ding, and Q. J. Zhang, "Efficient analytical formulation and sensitivity analysis of neuro-space mapping for nonlinear microwave device modeling," *IEEE Trans. Microw. Theory Techn.*, Vol. 53, No. 9, 2752–2767, Sep. 2005.
30. Bakr, M. H., J. W. Bandler, M. A. Ismail, J. E. Rayas-Sanchez, and Q. J. Zhang, "Neural space-mapping optimization for EM-based design," *IEEE Trans. Microw. Theory Techn.*, Vol. 48, No. 12, 2307–2315, Dec. 2000.
31. Gutierrez-Ayala, V. and J. E. Rayas-Sanchez, "Neural input space mapping optimization based on nonlinear two-layer perceptrons with optimized nonlinearity," *Int. J. RF Microw. Comput.-Aided Eng.*, Vol. 20, No. 5, 512–526, Sep. 2010.
32. Feng, F. and Q. J. Zhang, "Neural space mapping optimization for EM design," *Proc. Asia-Pacific Microw. Conf.*, 1–3, Nanjing, China, Dec. 2015.
33. Gorissen, D., L. Zhang, Q. J. Zhang, and T. Dhaene, "Evolutionary neuro-space mapping technique for modeling of nonlinear microwave devices," *IEEE Trans. Microw. Theory Techn.*, Vol. 59, No. 2, 213–229, Feb. 2011.
34. Koziel, S., J. W. Bandler, and K. Madsen, "A space mapping framework for engineering optimization: Theory and implementation," *IEEE Trans. Microw. Theory Techn.*, Vol. 54, No. 10, 3721–3730, Oct. 2006.
35. Koziel, S., J. W. Bandler, and Q. S. Cheng, "Tuning space mapping design framework exploiting reduced electromagnetic models," *IET Microw. Antennas Propag.*, Vol. 5, No. 10, 1219–1226, Jul. 2011.
36. Meng, J., S. Koziel, J. W. Bandler, M. H. Bakr, and Q. S. Cheng, "Tuning space mapping: A novel technique for engineering design optimization," *IEEE MTT-S Int. Microw. Symp. Dig.*, 991–994, Atlanta, Georgia, Jun. 2008.
37. Zhang, C., F. Feng, and Q. J. Zhang, "EM optimization using coarse and fine mesh space mapping," *Proc. Asia-Pacific Microw. Conf.*, 824–826, Seoul, Korea, Dec. 2013.
38. Feng, F., C. Zhang, V. M. R. Gongal-Reddy, and Q. J. Zhang, "Knowledge-based coarse and fine mesh space mapping approach to EM optimization," *Int. Conf. Numerical Electromagnetic Modeling and Optimization*, 1–4, Pavia, Italy, May 2014.
39. Koziel, S., S. Ogurtsov, J. W. Bandler, and Q. S. Cheng, "Reliable space-mapping optimization integrated with EM-based adjoint sensitivities," *IEEE Trans. Microw. Theory Techn.*, Vol. 61, No. 10, 3493–3502, Oct. 2013.
40. Koziel, S., Q. S. Cheng, and J. W. Bandler, "Fast EM modeling exploiting shape-preserving response prediction and space mapping," *IEEE Trans. Microw. Theory Techn.*, Vol. 62, No. 3, 399–407, Mar. 2014.
41. Feng, F., V. M. R. Gongal-Reddy, C. Zhang, W. Na, S. Zhang, and Q. J. Zhang, "Recent advances in parallel EM optimization approaches," *IEEE MTT-S Int. Conf. Microw. Millimeter Wave Technology*, 1–3, Beijing, China, Jun. 2016.
42. Feng, F., V. M. R. Gongal-Reddy, S. Zhang, and Q. J. Zhang, "Recent advances in space mapping approach to EM optimization," *Proc. Asia-Pacific Microw. Conf.*, 1–3, Nanjing, China, Dec. 2015.
43. Garcia-Lamperez, A., S. Llorente-Romano, M. Salazar-Palma, and T. K. Sarkar, "Efficient electromagnetic optimization of microwave filters and multiplexers using rational models," *IEEE Trans. Microw. Theory Techn.*, Vol. 52, No. 2, 508–521, Feb. 2004.

44. Garcia-Lamperez, A. and M. Salazar-Palma, "Multilevel aggressive space mapping applied to coupled-resonator filters," *IEEE MTT-S Int. Microw. Symp. Dig.*, 1–4, San Francisco, CA, May 2016.
45. Feng, F., C. Zhang, V. M. R. Gongal-Reddy, Q. J. Zhang, and J. Ma, "Parallel space-mapping approach to EM optimization," *IEEE Trans. Microw. Theory Techn.*, Vol. 62, No. 5, 1135–1148, Apr. 2014.
46. Tu, S., Q. S. Cheng, Y. Zhang, J. W. Bandler, and N. K. Nikolova, "Space mapping optimization of handset antennas exploiting thin-wire models," *IEEE Trans. Antennas Propag.*, Vol. 61, No. 7, 3797–3807, Jul. 2013.
47. Cao, Y., G. Wang, and Q.-J. Zhang, "A new training approach for parametric modeling of microwave passive components using combined neural networks and transfer functions," *IEEE Trans. Microw. Theory Techn.*, Vol. 57, No. 11, 2727–2742, Nov. 2009.
48. Feng, F., C. Zhang, J. Ma, and Q.-J. Zhang, "Parametric modeling of EM behavior of microwave components using combined neural networks and pole-residue-based transfer functions," *IEEE Trans. Microw. Theory Techn.*, Vol. 64, No. 1, 60–77, Jan. 2016.
49. Feng, F., V.-M.-R. Gongal-Reddy, C. Zhang, J. Ma, and Q.-J. Zhang, "Parametric modeling of microwave components using adjoint neural networks and pole-residue transfer functions with EM sensitivity analysis," *IEEE Trans. Microw. Theory Techn.*, Vol. 65, No. 6, 1955–1975, Jun. 2017.
50. Gongal-Reddy, V.-M.-R., S. Zhang, C. Zhang, and Q.-J. Zhang, "Parallel computational approach to gradient based EM optimization of passive microwave circuits," *IEEE Trans. Microw. Theory Techn.*, Vol. 64, No. 1, 44–59, Jan. 2016.
51. Gongal-Reddy, V.-M.-R., F. Feng, C. Zhang, S. Zhang, and Q.-J. Zhang, "Parallel decomposition approach to gradient-based em optimization," *IEEE Trans. Microw. Theory Techn.*, Vol. 64, No. 11, 3380–3399, Nov. 2016.
52. Koziel, S., "Shape-preserving response prediction for microwave design optimization," *IEEE Trans. Microw. Theory Techn.*, Vol. 58, No. 11, 2829–2837, Nov. 2010.
53. Zhang, C., F. Feng, V.-M.-R. Gongal-Reddy, Q. J. Zhang, and J. W. Bandler, "Cognition-driven formulation of space mapping for equal-ripple optimization of microwave filters," *IEEE Trans. Microw. Theory Techn.*, Vol. 63, No. 7, 2154–2165, Jul. 2015.
54. Zhang, C., F. Feng, Q. Zhang, and J. W. Bandler, "Enhanced cognition-driven formulation of space mapping for equal-ripple optimisation of microwave filters," *IET Microw., Antennas Propag.*, Vol. 12, No. 1, 82–91, Dec. 2018.
55. Feng, F., C. Zhang, S. Zhang, V.-M.-R. Gongal-Reddy, and Q.-J. Zhang, "Parallel EM optimization approach to microwave filter design using feature assisted neuro-transfer functions," *2016 IEEE/MTT-S International Microwave Symposium — MTT 2016*, 1–3, IEEE, San Francisco, CA, USA, May 2016.
56. Feng, F., W. Na, W. Liu, S. Yan, L. Zhu, and Q.-J. Zhang, "Parallel gradient-based em optimization for microwave components using adjoint-sensitivity-based neuro-transfer function surrogate," *IEEE Trans. Microw. Theory Techn.*, Vol. 68, No. 9, 3606–3620, Sep. 2020.
57. Feng, F., W. Na, W. Liu, S. Yan, L. Zhu, J. Ma, and Q.-J. Zhang, "Multifeature-assisted neuro-transfer function surrogate-based EM optimization exploiting trust-region algorithms for microwave filter design," *IEEE Trans. Microw. Theory Techn.*, Vol. 68, No. 2, 531–542, Feb. 2020.
58. Gustavsen, B. and A. Semlyen, "Rational approximation of frequency domain responses by vector fitting," *IEEE Trans. Power Deliv.*, Vol. 14, 1052–1061, Jul. 1999.